Colloidal quantum-dot light-emitting diodes with metal-oxide charge transport layers

J. M. CARUGE[1†], J. E. HALPERT[1†], V. WOOD[2†], V. BULOVIĆ[2*] AND M. G. BAWENDI[1]

[1]Department of Chemistry, Massachusetts Institute of Technology, Cambridge, Massachusetts 02139, USA
[2]Department of Electrical Engineering, Massachusetts Institute of Technology, Cambridge, Massachusetts 02139, USA
[†]These authors contributed equally to this work.
*e-mail: bulovic@mit.edu

Published online: 16 March 2008; doi:10.1038/nphoton.2008.34

Colloidal quantum dots, with their tunable luminescence properties, are uniquely suited for use as lumophores in light-emitting devices for display technologies and large-area planar lighting[1–10]. In contrast to epitaxially grown quantum dots, colloidal quantum dots can be synthesized as highly monodisperse colloids and solution deposited over large areas into densely packed, solid-state multilayers, which have shown promise as efficient optical gain media[11]. To be a viable platform for colour-tunable electrically pumped lasers, the present-generation quantum-dot LEDs must be modified to withstand the extended, high-current-density operation needed to achieve population inversion. This requirement necessitates a quantum-dot LED design that incorporates robust charge transport layers. Here we report the use of sputtered, amorphous inorganic semiconductors as robust charge transport layers and demonstrate devices capable of operating at current densities exceeding 3.5 A cm^{-2} with peak brightness of 1,950 Cd m^{-2} and maximum external electroluminescence efficiency of nearly 0.1%, which represents a 100-fold improvement over previously reported structures[8,10].

Previous efforts at building colloidal quantum-dot (QD) LEDs with inorganic charge transport layers have demonstrated only limited quantum dot (QD) electroluminescence (EL) efficiency. One study placed a multilayer of QDs between indium tin oxide (ITO) and silver electrodes[10]. The low luminescence efficiency (10^{-3} Cd A^{-1}) of these structures could be attributed to a number of sources, including luminescence quenching of the QDs by plasmon modes in the highly conductive electrodes[12], luminescence quenching by QD charging[13], or low efficiency due to imbalance in the polarity of charges injected into the device, which could lead to excess background current[14]. More recent work using doped GaN transport layers surrounding colloidal QDs reported external quantum efficiencies (EQEs) of 0.001–0.01%, although much of the observed EL arose from the GaN (ref. 8). These devices exhibited non-uniform emission across the pixel area, and fabrication required the specialized deposition technique of energy-neutral atomic-beam lithography or epitaxy. In contrast to this early attempt, in the present work we demonstrate the first general method that reproducibly fabricates patterned, all-inorganic optoelectronic devices with functional QD lumophores. We use amorphous, radiofrequency (RF)-sputtered metal oxides as QD-LED charge transport layers, deposited at room temperature to be broadly compatible with colloidal QDs and many other constituent films. With this advance, all-inorganic, QD-containing devices can, for the first time, be systematically engineered, as exemplified by our demonstration of QD-LEDs that manifest 100-fold higher EQEs than previously reported all-inorganic colloidal QD-LED structures.

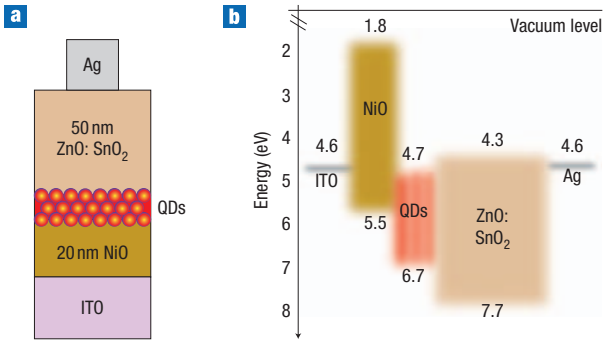

Figure 1 Quantum-dot light-emitting diode design. a, Schematic of the device structure showing the ITO anode, the Ni HTL, the QD active luminescent layer, the $ZnO:SnO_2$ ETL and the silver cathode. **b**, A band diagram determined from UV photoemission spectroscopy and optical absorption measurements, giving the approximate electron affinities and ionization energies of the QD-LED materials.

We follow three main guidelines in the choice and preparation of the metal oxide charge transport layers. First, we chose mechanically smooth and compositionally amorphous films to prevent electrical shorts or the formation of preferred current channels through the device structure. Second, we grew semiconducting oxide films with low free-carrier concentrations to minimize quenching of the QD EL through free-carrier plasmon modes. Third, the hole transport layer (HTL) and the electron transport layer (ETL) were chosen to have similar free-carrier concentrations and energy-band offsets to the QDs so that electron and hole injection into the QD layer was balanced. An excess of one type of carrier in the QD region results in QD

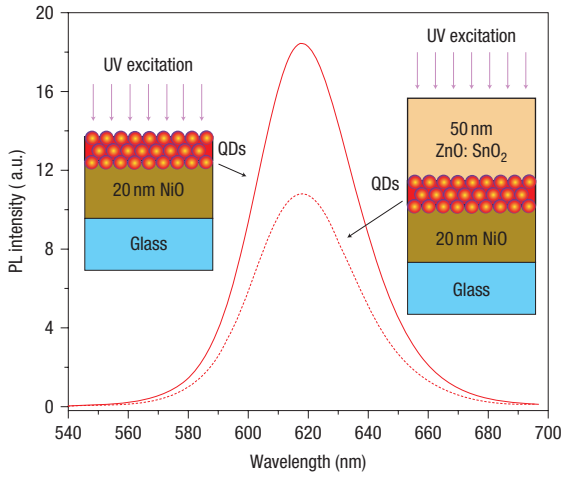

Figure 2 Effect of ZnO:SnO_2 layer deposition. Photoluminescence spectra before (solid line) and after (dotted line) deposition of a 50-nm-thick ZnO:SnO_2 layer onto ZnCdSe QDs on NiO. All the materials were deposited with the same conditions used for device fabrication, although this QD batch had a slightly different peak emission wavelength. Both samples were excited within the same optical geometry using a UV lamp. We measured a 40% drop in the PL intensity on average.

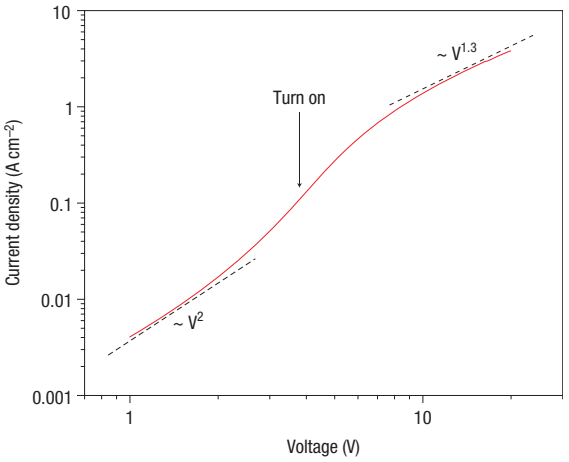

Figure 3 Quantum-dot light-emitting diode current–voltage characteristics. Current density versus voltage log–log plot for the QD-LED of Fig. 1a. Three different regimes of conduction are clearly visible. At low voltages the device shows space-charge-limited conduction. At 3 V, the slope of the *J*–*V* plot increases as both holes and electrons are injected into the QD, and the onset of EL is observed at 3.8 V. At higher *V*, the *J*–*V* behaviour tends to ohmic conduction.

charging, which increases the likelihood of non-radiative three-body Auger relaxations[12] and therefore decreases EL efficiency. These requirements highlight the important benefits in using metal oxides as versatile charge transport layers; metal oxides offer a range of deposition-determined morphologies as well as tunable conductivities and adjustable ionization energies through doping and physical co-deposition.

The cross-section of our QD-LED is depicted in Fig. 1a with the approximate electronic band structure of constituent layers shown in Fig. 1b. Following our previous work on hybrid organic–inorganic QD-LED structures[1], the HTL of the present QD-LEDs was a 20-nm-thick film of NiO deposited on ITO. The resistivity of the NiO film was tuned to 5 Ωcm by adjusting the oxygen concentration in the Ar:O_2 plasma during the RF magnetron sputtering process[15,16]. Hot-probe and X-ray-diffracted measurements indicate that as-grown NiO films are amorphous and p-type. Atomic force microscope (AFM) characterization of the NiO layer on top of the ITO electrodes revealed a root-mean-square roughness of <0.5 nm, which enables deposition of smooth monolayers of self-assembled QDs onto the NiO.

The luminescence layer of QD-LEDs consisted of ZnCdSe alloyed QDs with an emission peak at wavelength $\lambda = 638$ nm, a full-width at half-maximum (FWHM) of 40 nm, and a colloidal solution photoluminescence (PL) quantum yield of $50 \pm 10\%$. The thin-film photoluminescence efficiency is lower by an order of magnitude. The QDs were spin-coated onto the NiO substrate so as to form a 30 ± 5 nm film consisting of from 3 to 4 close-packed QD monolayers. We chose ZnCdSe cores over more traditional CdSe/ZnS core/shell QDs owing to their ease of production and because ZnCdSe alloyed QDs, which are not overcoated with a wide-bandgap ZnS layer, should enable easier charge injection into the QDs. In this study, our highest EL efficiencies were measured for QD-LEDs containing ZnCdSe QDs; however, devices containing CdSe/ZnS QDs show efficiencies within an order of magnitude.

For the ETL, we selected a 50-nm-thick, optically transparent film of alloyed ZnO and SnO_2, with a resistivity of 10 Ω cm. ZnO:SnO_2 alloy is an n-type semiconductor and, as shown schematically in Fig. 1b, its conduction-band level allows injection of electrons into the ZnCdSe QD conduction band. Whereas pure ZnO or SnO_2 films tend to be polycrystalline with pronounced grain boundaries, AFM and X-ray diffraction measurements indicate that ZnO:SnO_2 films are relatively smooth (with < 0.5 nm r.m.s. roughness) and crystallographically amorphous, reducing the likelihood of morphologically induced electrical shorts in the device. Our choice of ZnO:SnO_2 also reflects the requirement that the ETL be sputtered directly onto the QDs without damaging them. Introducing O_2 into the sputtering gas, as with NiO, could oxidize the organic ligands capping the QDs and produce trap sites that facilitate non-radiative recombination of QD excitons. The ZnO:SnO_2 ratio determines the film conductivity, eliminating the need for excess oxygen in the sputtering process. To determine whether the ZnO:SnO_2 deposition causes physical damage to the QDs, we compared the UV-excited PL intensity from QDs on NiO and from QDs embedded in a NiO/QD/ZnO:SnO_2 structure. As shown in Fig. 2, we observed a 40% drop in intensity as a result of the ZnO:SnO_2 deposition, which indicates that sputtering the ETL on the QDs largely preserves the passivating ligands. In fact, much of the decrease in QD luminescence can be attributed to additional quenching by the free carriers in the ETL. A silver cathode was chosen to allow electron injection into the conduction band of the ZnO:SnO_2 layer.

All our QD-LEDs were tested in air over several days. The devices were tested as-made, without additional environmental packaging, and were stored in atmospheric conditions between experiments. Figure 3 shows the forward biased current density versus voltage (J–V) log–log plot for the QD-LED described above. The J–V slope with a gradient of two between 1 V and 3 V is indicative of space-charge-limited conduction for one of the carriers. The increase in the J–V slope at 3 V coincides with

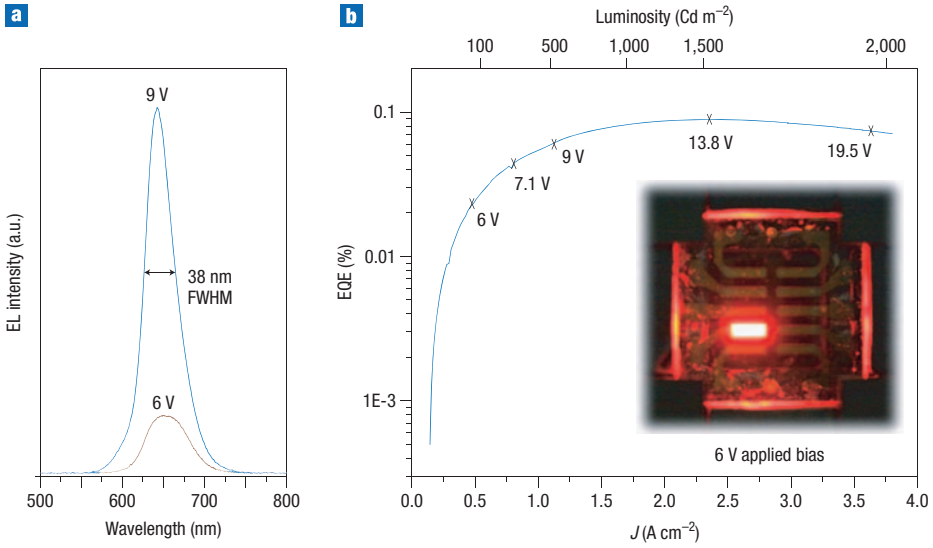

Figure 4 Quantum-dot light-emitting diode EL spectrum and efficiency. a, Electroluminescence spectra of the QD-LED of Fig. 1a at 6 V (0.46 A cm^{-2}) and 9 V (1.14 A cm^{-2}) applied bias. **b**, Plot of the QD-LED EQE measured from the front face of the device as a function of *J*. A maximum EQE of 0.09% and a luminance of 1,500 Cd m^{-2} were reached at 13.8 V, 2.33 A cm^{-2}. The inset shows a photograph of a bright and uniform pixel at 6 V applied bias. A significant amount of additional light was guided through the glass substrate and emitted at the four substrate edges, as is evident from the photograph. The presence of the edge-emitted light is not reflected in the stated EQE measurements.

the onset of QD-LED EL, which is first observed at 3.8 V, and is therefore associated with the onset of both electron and hole injection into the QDs. The elevated current and J–V slope of 1.3 for applied voltages greater than 10 V is a signature of the combined J–V characteristics for injected electrons and holes, with one or both of the carriers tending to ohmic conduction. These QD-LEDs sustain steady-state current densities of up to 3.5 A cm^{-2}, which corresponds to a carrier injection rate of 1×10^7 carriers per second per QD and a maximum exciton density per QD of 0.1.

Figure 4a shows a characteristic QD EL peak centred at $\lambda = 642$ nm with a FWHM of 38 nm. The similarity between the EL spectrum and the PL of QDs in solution (FWHM = 40 nm) indicates that the device emission is due entirely to the QDs. Figure 4b shows the EQE of the QD-LED as a function of J, which, at its maximum of 0.09%, is almost two orders of magnitude higher than previous reports of devices with QDs embedded between doped inorganic transport layers[8]. At 6 V, 0.46 A cm^{-2}, pixel brightness is uniform at 74 Cd m^{-2}, with emission entirely from the QDs. Standard video brightness (200 Cd m^{-2}) occurs in our device at 7.15 V, 0.71 A cm^{-2}. The peak brightness is measured to be 1,950 Cd m^{-2} when J is 3.73 A cm^{-2} (19.5 V), and the peak luminescence efficiency is 0.064 Cd A^{-1} when J is 2.33 A cm^{-2} (13.8 V). Comparable brightness and J–V characteristics were observed when the devices were tested after being stored in air for four days, in contrast to unpackaged organic QD-LEDs, which cannot withstand prolonged atmospheric exposure. The EQE of the QD-LED reported here is probably limited by Förster energy transfer between QDs and Auger recombination due to QD charging, which results from electron energy-band alignment of the constituent QD-LED layers. The QD-LED response to sinusoidally modulated drive voltage is plotted in Fig. 5, with the amplitude of the modulation in the light output showing a 3-dB frequency of 1.2 MHz, corresponding to a QD-LED response faster than 1 μs.

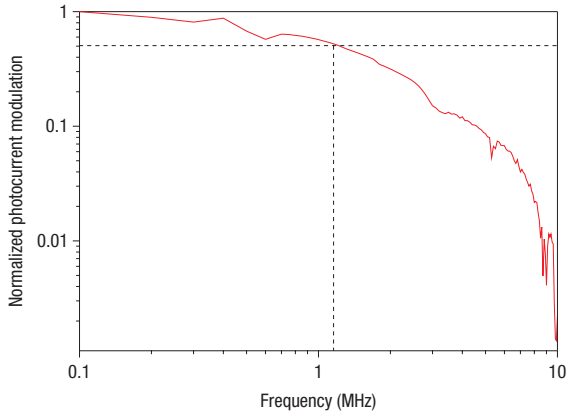

Figure 5 Quantum-dot light-emitting diode RC time-constant measurement. Plot of the modulation in QD-LED EL intensity (noted as the normalized photocurrent in the EL photodetector) operated at $V = V_{dc} + V_m \sin(\omega t)$, with $V_{dc} = 9$ V, $V_m = 5$ V and ω indicated on the abscissa. The half-power point of the curve corresponds to the 3-dB cutoff frequency of 1.2 MHz.

To study the exciton dynamics in our devices and determine whether electrically pumped lasing of QDs in QD-LED structures is feasible, we performed time-resolved PL measurements on the charge transport layers and the QDs. No PL signal was measured from optically excited 50-nm-thick NiO and ZnO:SnO_2 thin films, indicating that non-radiative processes faster than 10 ps dominate exciton relaxation in the metal-oxide transport layers. This implies that the dominant mechanism for generating EL in our QD-LEDs was direct charge injection into the QD layer rather than energy transfer from weakly bound metal-oxide Wannier excitons to excitons in the QDs. To achieve biexciton lasing in colloidal QD films, the exciton generation rate must

compete with non-radiative processes such as the Auger decay[11,13]. With time-resolved PL we measured a biexciton lifetime of 1.3 ns for the CdZnSe QDs. Therefore, for the onset of the biexciton lasing action an average charge-carrier injection rate of nearly 1×10^9 electrons per second per QD is needed, which is 100 times higher than the maximum steady-state J obtained in this study. To reach the elevated current densities that might lead to lasing action, the QD-LEDs could be run in pulsed mode, as previously demonstrated in experiments with organic LEDs ref. 17. Note that additional optical absorption due to proposed high carrier density in the QD layers[18] might necessitate even larger drive currents, which further emphasizes the need for robust inorganic devices as the first step in the demonstration of electrically pumped colloidal QD lasers.

In conclusion, this work demonstrates that metal oxides and colloidal QDs can be combined to fabricate bright, monochrome LEDs with uniform pixel emission of saturated colour and high peak luminance. The brightness of the devices reported here matches that of the best organic-based QD-LEDs, but with the benefit of improved shelf-life robustness inherent in the environmental stability of metal-oxide charge transport layers. The stable operation under a high carrier-injection rate should enable evolution of the QD-LEDs to device designs that will be needed to demonstrate electrically pumped colloidal QD lasers. Such devices would be able to take full advantage of the tunability and the ease of fabrication and processing of colloidal QDs to provide simple, tunable, coherent light sources.

METHODS

METAL OXIDE AND QUANTUM DOT CHARACTERIZATION

Atomic-force-microscope characterizations of the metal oxide and QD thin films were done with the Digital Instruments Dimension 3000 in the tapping mode. X-ray diffraction measurements were performed with the Rigaku Powder 250 mm diffractometer. Hot-point probe measurements to determine the semiconductor type involved a standard multimeter with one contact heated using a soldering iron.

COLLOIDAL QUANTUM-DOT LIGHT-EMITTING DIODE FABRICATION

To fabricate a colloidal QD-LED, cleaned glass substrates were patterned with a 60-nm-thick ITO anode deposited through a shadow mask using RF magnetron sputtering in an inert argon environment at a pressure of 5 mtorr and a rate of 0.06 Å s^{-1}. The substrate was heated to ~250 °C during deposition to increase the ITO conductivity. The slow growth rate prevents surface roughness on the ITO electrode, which can induce roughness in the HTL, leading to electrical shorts through the device structure. The 20-nm-thick, p-type, NiO HTL was sputtered onto the ITO at a deposition rate of 0.2 Å s^{-1} in a 2:100 oxygen to argon atmosphere at a pressured 6 mtorr pressure and using 200 W of RF power.

Building on earlier work[19,20], the colloidal QDs were synthesized by injecting trioctylphosphine selenide into a pot of ZnO, CdO, oleic acid and 1-octadecene at 310 °C. The ZnCdSe QDs were precipitated twice with acetone and redispersed in chloroform. The correct concentration of QD solution to yield three to four layers of QDs on the NiO was approximated using optical absorption measurements and confirmed using an AFM. Quantum dots were spin-deposited onto the NiO in a nitrogen atmosphere.

The ETL was deposited on the QDs by simultaneously sputtering ZnO at 15 W and SnO_2 at 9 W in a pure argon environment at a pressure of 5 mtorr. This corresponds to a combined deposition rate of 0.2 Å s^{-1}, which is sufficiently slow to minimize damage to the QD underlayer. A 40-nm-thick silver cathode was then thermally evaporated through a shadow mask onto the ZnO:SnO_2 at a rate of 1.5 Å s^{-1}.

Each 12 mm × 12 mm substrate was patterned to yield 10 devices, each with an area of 0.012 cm^2.

COLLOIDAL QUANTUM-DOT LIGHT-EMITTING DIODE CHARACTERIZATION

Our devices were measured without environmental packaging and in atmospheric conditions. Current–voltage characteristics of the QD-LED were recorded using a computer-controlled Keithley 2612 current/voltage source meter. To calculate the EQEs, the EL from the front face of the device was detected using a calibrated Newport 2112 silicon photodetector at the same time that the J–V characteristics were measured. Electroluminescence spectra were taken with an Ocean Optics spectrometer with bias applied to the device using the Keithley 2612.

To calculate the exciton density per QD in a hexagonally close-packed film, we used the measured current density and approximated the QD cross-sectional area. We assumed equal hole and electron currents and that all charge carriers flow through the QDs and not the ligands. We used a QD lifetime of 5 ns in a close-packed film, a QD radius of 4 nm, and a ligand length of 1 nm.

For the time-resolved PL measurements, samples were excited with 100-fs-long optical pulses with a wavelength of 400 nm, generated by a Ti:sapphire regenerative laser amplifier with a frequency doubler. The PL was detected with a 10-ps resolution streak camera. The biexciton lifetimes were calculated as described in ref. 18.

The resistance–capacitance (RC) time constant of the device was measured by applying a fixed d.c. bias, V_{dc}, to the device using a Keithley 2612 and a sinusoidal modulated voltage, V_m, using an Agilent 33250A waveform generator, such that the total applied voltage was given by $V = V_{dc} + V_m \sin(\omega t)$. The angular frequency, ω, was varied, and the decrease in the modulation of the EL intensity was detected as described above.

Received 21 August 2007; accepted 17 January 2008; published 16 March 2008.

References

1. Caruge, J.-M., Halpert, J. E., Bulović, V. & Bawendi, M. G. NiO as an inorganic hole-transporting layer in quantum-dot light emitting devices. *Nano Lett.* **6,** 2991–2994 (2006).
2. Coe, S., Woo, W. K., Bawendi, M. & Bulović, V. Electroluminescence from single monolayers of nanocrystals in molecular organic devices. *Nature* **420,** 800–803 (2002).
3. Coe-Sullivan, S., Steckel, J. S., Woo, W. K., Bawendi, M. G. & Bulović, V. Large-area ordered quantum-dot monolayers via phase separation during spin-casting. *Adv. Funct. Mater.* **15,** 1117–1124 (2005).
4. Coe-Sullivan, S., Woo, W. K., Steckel, J. S., Bawendi, M. G. & Bulović, V. Tuning the performance of hybrid organic/inorganic quantum dot light-emitting devices. *Organic Electron.* **4,** 123–130 (2003).
5. Schlamp, M., Peng, X. & Alivisatos, A. P. Improved efficiencies in light emitting diodes made with CdSe(CdS) core/shell type nanocrystals and a semiconducting polymer. *J. Appl. Phys.* **82,** 5837–5842 (1997).
6. Steckel, J. S. *et. al.* Blue luminescence from (CdS)ZnS core–shell nanocrystals. *Angew. Chem. Int. Edn* **43,** 2154–2158 (2004).
7. Zhao, J. *et al.* Efficient CdSe/CdS quantum dot light-emitting diodes using a thermally polymerized hole transport layer. *Nano Lett.* **6,** 463–467 (2006).
8. Mueller, A. H. *et al.* Multicolor light-emitting diodes based on semiconductor nanocrystals encapsulated in GaN charge injection layers. *Nano Lett.* **5,** 1039–1044 (2005).
9. Colvin, V. L., Schlamp, M. C. & Alivisatos, A. P. Light-emitting diodes made from cadmium selenide nanocrystals and a semiconducting polymer. *Nature* **370,** 354–357 (1994).
10. Hikmet, R. A. M., Talapin, D. V. & Weller, H. Study of conduction mechanism and electroluminescence in CdSe/ZnS quantum dot composites. *J. Appl. Phys.* **93,** 3509–3514 (2003).
11. Klimov, V. I. *et. al.* Optical gain and stimulated emission in nanocrystal quantum dots. *Science* **290,** 314–317 (2000).
12. Shimizu, K. T., Woo, W. K., Fisher, B. R., Eisler, H. J. & Bawendi, M. G. Surface-enhanced emission from single semiconductor nanocrystals. *Phys. Rev. Lett.* **89,** 117401 (2002).
13. Klimov, V. I., Mikhailovsky, A. A., McBranch, D. W. & Bawendi, M. G. Quantization of multiparticle auger rates in semiconductor quantum dots. *Science* **287,** 1011–1013 (2000).
14. Malliaras, G. G. & Scott, J. C. The roles of injection and mobility in organic light emitting diodes. *J. Appl. Phys.* **83,** 5399–5403 (1998).
15. Yamada, S., Yoshioka, T., Miyashita, M., Urabe, K. & Kitao, M. Electrochromic properties of sputtered nickel oxide. *J. Appl. Phys.* **63,** 2116–2119 (1987).
16. Yoshimura, K., Miki, T. & Tanemura, S. Nickel oxide electrochromic thin films prepared by reactive dc magnetron sputtering. *Jpn J. Appl. Phys.* **34,** 2440–2446 (1995).
17. Kozlov, V. G. *et al.* Structures for organic diode lasers and optical properties of organic semiconductors under intense optical and electrical excitations. *IEEE J. Quant. Electron.* **36,** 18–26 (2000).
18. Fisher, B. R., Caruge, J.-M., Chan, Y. T., Halpert, J. E. & Bawendi, M. G. Multiexciton fluorescence from semiconductor nanocrystals. *Chem. Phys.* **318,** 71–81 (2005).
19. Zhong, X., Feng, Y., Knoll, W. & Han, M. Alloyed $Zn_xCd_{1-x}S$ nanocrystals with highly narrow luminescence spectral width. *J. Am. Chem. Soc.* **125,** 13559–13563 (2003).
20. Zhong, X., Han, M., Dong, Z., White, T. J. & Knoll, W. Composition-tunable $Zn_xCd_{1-x}Se$ nanocrystals with high luminescence and stability. *J. Am. Chem. Soc.* **125,** 8589–8594 (2003).

Acknowledgements

The authors would like to thank G. Nair and G. Chen for their technical assistance and P. Mardilovich for insightful discussions. This work was supported in part by the National Science Foundation Materials Research Science and Engineering Center at (NSF-MRSEC) the Massachusetts Institute of Technology (MIT) Program (DMR-0213282), making use of its Shared Experimental Facilities, the Harrison Spectroscopy Laboratory (NSF-CHE-011370), the U.S. Army through the Institute for Soldier Nanotechnologies (DAAD-19-02-0002), National Science Foundation Nanoscale Interdisciplinary Research Team (NSF NIRT) (CHE-0507147), and a Presidential Early Carrier Award for Scientists and Engineers (PECASE).

Correspondence and requests for materials should be addressed to V.B.